8-16-2004

Modeling Concrete Masonry Walls Subjected To Explosive Loads

Christopher D. Eamon
Mississippi State University, Starkville, MS, christopher.eamon@wayne.edu

James T. Baylot
US Army Engineering Research and Development Center, Vicksburg, MS

James L. O'Daniel
US Army Engineering Research and Development Center, Vicksburg, MS

MODELING CONCRETE MASONRY WALLS SUBJECTED TO EXPLOSIVE LOADS

Christopher D. Eamon, M.ASCE[1], James T. Baylot, F..ASCE[2], and James L. O'Daniel, A.M.ASCE[3]

ABSTRACT

Concrete masonry unit walls subjected to blast pressure were analyzed with the finite element method, with the goal of developing a computationally-efficient and accurate model. Wall behavior can be grouped into three modes of failure, which correspond to three ranges of blast pressures. Computational results were compared to high-speed video images and debris velocities obtained from experimental data. A parametric analysis was conducted to determine the sensitivity of computed results to critical modeling values. It was found that the model has the ability to replicate experimental results with good agreement. However, it was also found that, without knowledge of actual material properties of the specific wall to be modeled, computational results are not reliable predictors of wall behavior.

INTRODUCTION

The exterior frames of many buildings are commonly in-filled with concrete masonry unit (CMU) blocks. In a typical high-energy blast in close proximity to this type of wall, the CMUs may break apart and enter the structure as projectiles, potentially injuring building occupants. The accurate prediction of this behavior is a subject of great interest in protective technology research, in order to evaluate the performance of

[1] Dept. of Civil Eng. Mississippi State University, Starkville, MS. E-mail: eamon@engr.msstate.edu
[2]US Army Eng. Research and Development Center, Vicksburg, MS. E-mail: James.T.Baylot@erdc.usace.army.mil
[3]US Army Eng. Research and Development Center, Vicksburg, MS. E-mail: James.L.O'Daniel@erdc.usace.army.mil

existing structures and to suggest appropriate retrofit options or designs for new structures.

A rigorous description of this behavior requires a highly nonlinear, large strain, large displacement approach that allows arbitrary element contact and separation. Compounded with uncertainties in load and material properties, the accurate modeling of CMU wall behavior subjected to blast loads is a difficult problem to solve. These analytical complexities are traditionally avoided by using empirical design rules based on experience and experimental evidence (DOE 1992). Associated with these empirical rules, however, are significant inaccuracies, particularly when new geometry, material, construction, or blast variables are present. To avoid these problems, a number of researchers have analytically replicated CMU wall behavior, typically with the finite element (FE) method. Some of these investigators have included Forsen (1985), Bogosian (1997), Murray (1997), and Dennis et al (2001).

To further understand the problem, and to provide data for future FE work, the US Army Engineer Research and Development Center (ERDC) recently conducted a sequence of experiments where quarter-scale models of CMU infill walls, held in rigid frames, were subjected to blast loads of various magnitudes (Dennis 2001). Many of these blasts failed the walls, which typically broke into multiple pieces. These wall fragments then flew through the air with various velocities.

Previous modeling efforts did not achieve the desired level of accuracy. Although some of the data can be replicated reasonably well with existing techniques, in many cases, particularly those at higher blast pressures, incorrect failure modes were obtained,

where walls broke in incorrect places, into an incorrect number of pieces, and with incorrect debris orientation.

It was the aim of this research, which builds from the work of Dennis et al. (2001), to resolve some of these shortcomings. The focus is to develop a computationally-efficient model that can replicate with reasonable accuracy the wall failure mechanisms and debris velocity of CMU walls subjected to blast loads.

EXPERIMENTAL DATA

Data from fourteen wall specimens were considered for modeling. The walls were constructed of ¼-scale size 203 by 203 by 406 mm (nominal 8 by 8 by 16 in) CMU blocks, as shown in Figure 1. The average ¼-scale CMU mass was 252g. Walls were 15 courses tall and 15.5 blocks wide. A 3.2 mm gap (at ¼ scale) was left between the top and sides of the wall edges and the rigid frame. A mortar joint was placed at the wall base. Walls tested were both ungrouted, where the hollow portions of the CMU blocks were left unfilled, and fully grouted, where voids were completely filled with grout. In all walls, a smooth 2.9 mm diameter steel dowel (equivalent to a #4 reinforcing bar at full scale) was placed in every third cell and rigidly connected to the top of the reaction frame. At the dowel location in the wall, the top cell was filled with grout but was not allowed to bond to the dowel, creating a 'slip-dowel' connection (Baylot et al. 2001). This connection was meant to represent the clips that connect non-load bearing, exterior infill walls to the structural frame of the building. Average grout and CMU strengths, based on compression tests conducted during the tests, were 15.9MPa. Material densities were 1700 kg/m^3 for the mortar and 1800 kg/m^3 for the CMU.

For each test, a charge of explosive material with weight deemed by the Army to be representative of a terrorist threat was placed at a particular distance from the wall, typically 3 m (equivalent to 12 m on the ¼ scale models), and detonated. During this time, blast pressure was recorded by five pressure gauges, located around the frame perimeter. The experimental set-up is shown in Figure 2. An example of a typical measured blast pressure curve, and the corresponding impulse, is shown in Figure 3. Accelerometers were also placed at mid-height and quarter-height of the wall (away from the blast side). Gauges sampled at a rate of 1000 kHz. The acceleration results were numerically integrated to obtain debris velocity readings. More important to this study, high-speed video recorded the behavior of the walls during the blast load. Load pressure magnitudes (and corresponding impulses), as well as the resulting wall response, can be divided into three categories, which are as follows:

1. High Pressure Case (two wall tests). Only the fully-grouted walls were subjected to this magnitude of pressure. These walls formed two horizontal break lines, failing in three large pieces, where the top and bottom thirds of the walls rotated inwards, while the central piece remained approximately vertical, as illustrated in Figure 4.

2. Moderate Pressure Case (two fully grouted tests, three ungrouted tests). Peak impulses were approximately ½ of the high pressure cases. The fully-grouted walls subjected to this pressure category failed in two large pieces. A single break line formed at mid-height and the two large pieces rotated inwards, as shown in Figure 5. The ungrouted

walls failed by breaking along nearly all horizontal mortar lines, with a peak deflection at the center of the wall, as shown in Figure 6.

3. Low Pressure Case (four fully grouted tests, three ungrouted tests). Peak impulses were approximately ¼ of the high pressure cases. Neither fully-grouted nor ungrouted walls subjected to this pressure collapsed, although some retained slight permanent deformations, as shown in Figure 7.

ANALYTICAL MODEL

Due to the time and cost constraints of the research program, the development of a specific FEA code for this project was infeasible. Therefore, DYNA3D, a large-strain, large-displacement Lagrangian nonlinear finite element code with an explicit (central difference) solver, was used for this study (LLNL 1999). The use of pre-packaged software, however, resulted in limitations (which are discussed later in this paper) that may have degraded results.

The basic element used was an 8-node hexahedral. The element is formulated with trilinear shape functions (constant strain), and the constitutive equations are evaluated based on the state at the center of the element. It is evaluated with an exact volume integration and based on the formulation by Flanagan and Belytschko (1981). Lumped mass matrices are used.

Given the constraints imposed on this study, it was necessary to develop a simple model that would minimize computational effort. Therefore, a number of reasonable

simplifications were made to reduce the complexity and cost of the analysis but still achieve reasonable modeling accuracy.

As the blast source was far enough away from the wall so that results from all pressure gauges were essentially the same, as shown in Figure 8, the average of this data was taken and applied as a time-varying, uniform pressure over the wall surface. To allow for manageable input, only several thousand data points were used of the nearly 100,000 in the recorded history. Load curves were decimated such that the resulting impulse curves had less than 1% error from the original at any point in the time history.

Since the vertical edges of the walls were not attached to the reaction structure, the walls generally responded as one-way systems, where the width of the wall does not significantly affect behavior, as shown throughout Figures 4-7. Therefore, walls were modeled as a single width column of 15 blocks stacked vertically. This model is shown in Figure 9. Although plane strain boundary conditions are an obvious choice for this model, the test data could not be successfully replicated with this assumption. Rather, modeling the wall with a single unit width and leaving the vertical edges free of constraints worked well. It is not clear why this is so. Possibly, small side-to-side displacements of the CMUs affect the failure behavior and must be accounted for.

The idealized CMUs are shown in Figure 10. They are 9.5 mm (3/8") taller and wider than the test blocks, as the standard mortar thickness of 9.5 mm is included into the CMU dimensions (width and height). The mortar itself is modeled as a zero-thickness contact surface, which is described in detail below. For ease of data input, since the idealized rectangular geometry does not match a standard 8 x 8 x 16 CMU, which contains sloping interior walls, such that the 'holes' on the top are slightly larger than

those on the bottom, there is a mass discrepancy (of about 10%). This is accounted for by adjusting the idealized block density accordingly, and results in an equivalent density of 1550 kg/m^3.

The CMU material law was taken as a Mohr-Coulomb failure surface with a Tresca limit, as shown in Figure 11. In this model, cohesion is taken as zero and friction angle is indirectly defined by the pressure-stress relationship given below, in accordance to the available experimental data (Dennis 2000). The shear modulus was taken as 5175MPa, while maximum principal stress at failure was 6.21MPa. Based on experimental data, the pressure-volume relationship for the CMUs is described with a simple equation of state that describes pressure as a linear function of volumetric strain:

$$p = -6.9X10^6 \varepsilon \qquad (1)$$

where p is pressure (kPa) and ε is volumetric strain. Until the Tresca limit, the pressure-stress relationship is also a linear function and is given by:

$$p = -0.05932 \sigma - 2632 \qquad (2)$$

where σ is stress (kPa). The model also assumes strengthening under higher (compressive) strain rates, which is shown by the curve in Figure 12. Material properties are taken from the literature (Beall 1995; ACI 1995; ASTM 1989; Virdee 1990)]. The strain rate strengthening curve is based on enhancements to compressive strength as reported in DOE/TIC 11268 (1992).

As the concern of this study is the modeling of the global failure and fragmentation behavior of the walls rather than the stress gradients within the CMU blocks, each of the fully-grouted CMUs were modeled with a single hexahedral element to minimize computational effort (with an exception being the very top and bottom

boundary blocks, to be discussed below). It was found that further refinement in mesh density did not significantly improve global results. This suggests that CMU interconnectivity and contact parameters along joint lines, rather than individual block deformations, govern global wall behavior (again, with the boundary blocks an exception). Clearly, however, this model would not be useful for determining stress gradations within individual CMUs. Ungrouted CMUs were modeled with a minimal number of elements as well, as shown in Figure 10.

The contact surface representing the mortar initially rigidly links adjoining blocks together. When a specified failure criterion is reached, the slide surface releases the nodal constraints, allowing the blocks to slide or separate and contact again arbitrarily. The failure criterion is given by equation 3:

$$\left(\frac{F_n}{F_{nf}}\right)^2 + \left(\frac{F_s}{F_{sf}}\right)^2 \geq 1 \qquad (3)$$

Where F_n and F_s are the calculated normal and shear stresses, respectively, while F_{nf} and F_{sf} are the allowable normal and shear stresses. Here F_s is equal to the vector sum of the two shear components on the interface surface. The failure stresses, based on experimental results (Dennis 2000), are taken as 2.76MPa for normal and 3.11MPa for shear stress for the high pressure cases, and 1.73MPa for normal and 2.21MPa for shear stress at the lower pressure cases. The failure stresses were increased for the higher blast pressure cases to represent mortar strengthening under higher strain rates, which could not otherwise be accounted for. Increases are based on expected material behavior provided from DOE/TIC 11268 (1992). The coefficients of friction between the block-block and block-frame interfaces vary widely in the literature (see, for example, the classic mechanics text by Seely and Ensign (1926), who report “stone-stone” values from

0.40 to 0.65 and “metal-stone” values from 0.30 to 0.70) and were initially taken as 0.50 for both the static and kinetic values.

In the modeling process, it was found to be necessary to model the top and bottom boundary blocks differently than the remaining CMUs. These two blocks were paired with a material model that allows element deactivation once a failure criterion is reached. For this model, elements that compose the boundary CMUs are deleted from the model during the solution process at a specified failure pressure. Here, failure pressure is taken to be 13.8MPa, based on experimental data previously collected (Dennis 2000). Otherwise, the model is similar to that used for the remaining CMUs.

It was found that this formulation was essential to properly capture the material crushing that occurs at the top and bottom CMUs, particularly at the higher load pressure cases. A special slide surface is specified between these CMU surfaces and the frame, that adapts to the new material boundary as failed elements are removed. Unfortunately, this approach is rather computationally intensive. However, it was found that modeling approaches leaving out this detail could not successfully replicate the various failure modes. The steel frame holding the top and bottom of the wall in place was modeled as rigid.

The slip-dowel was modeled with solid elements and extended into a cavity in the top CMU, where a small gap (an arbitrarily small value) was left between the surfaces of the CMU and dowel. If this gap were not provided and the contact surfaces laid directly on top of one another, numerical difficulties arose in the analysis and often led to non-convergence for the high load cases. Unfortunately, the use of simpler beam or shell

elements to model the dowel proved to be ineffective, as the special contact surface compatible with element deletion was not available for these element types.

The adaptive contact surface was specified on only one side of the dowel and the CMU, that facing away from the blast source, as shown in Figure 13. Specifying the contact surface on the other side of the rebar only increased computational effort but did not improve results, as contact here was minimal, if at all, in most cases.

The rebar was modeled with an elasto-plastic material model with standard steel properties, with yield of 345MPa. It was not possible to include strain-rate strengthening of the steel or of the top and bottom CMU blocks, again a limitation resulting from the use of the adaptive slide surface. It was found, however, that simulating material disintegration at the boundary blocks was the dominant factor contributing to correct failure behavior, rather than strain rate strengthening, particularly for the high pressure cases.

The meshes of the top and bottom blocks were refined to approximately 10 elements along each side, where the rebar was modeled with ten elements along its length and only one element through the thickness. It was found that this coarse mesh could adequately capture the wall behavior for the test cases, without unduly lengthening computational time.

RESULTS

The models correctly matched, in every case considered, which walls would remain intact (all of the low pressure cases) and which walls would fail (the moderate and

high pressure cases) using the base material parameter values given above. In this study, failure is defined as wall collapse.

However, for the walls that failed, the assumed material parameters would not model all test results accurately. In particular, it was found that wall failure behavior, especially at the high pressure blasts, was sensitive to variations in top block CMU failure strength and block-frame contact friction. The range of values that well-replicated all test results are given in Table 1. This table indicates that analysis results are more sensitive to parameter values at the higher blast pressure cases. Here, a wider range of frame-block friction and top block failure pressure was needed to accurately replicate experimental results, as compared to the lower-pressure cases were relatively insensitive to these values. It also appears that the frame-block friction coefficient is better taken as 0.65, which appears throughout the table, rather than the value of 0.50 which was initially assumed. This seems to better match values reported in the literature as well, which suggest a higher value of friction between the frame-block interface than the block-block interface (Seely & Ensign 1926; ACI 318-95 1995).

Figures 14-17 illustrate FE results for a typical wall exposed to: high pressure; moderate pressure (wall grouted); moderate pressure (wall ungrouted); and low pressure (wall ungrouted). These results should be compared to Figures 4-7, respectively, which are the corresponding experimental results. The FE solutions replicate the overall response of the walls well, generally matching failure shape, location of break lines, and size and number of primary pieces of debris. Peak debris velocities for the seven (of fourteen) walls that failed are shown together with the experimental data in Figure 18.

Detailed results of a sensitivity study are given in Tables 2-6, where various parameters were incremented, adjusted one at a time while holding others constant. Here, a typical wall from each of the five groups (high-pressure, grouted; moderate pressure, grouted; low pressure, grouted; moderate pressure, ungrouted; and low pressure, ungrouted) was analyzed considering changes in each of the following parameters: top block failure pressure ("Block Strength"); block-frame contact friction ("Frame Friction"); block-block contact slide-surface strength ("Mortar Strength"); block-block contact friction ("Block Friction") and blast pressure. Changes in failure mode as well as maximum debris velocity are noted. In the tables, the base parameter value is given and all incremented values are normalized to this value. Figures 19a-i, as referenced in Tables 2-6, illustrate the corresponding wall failure modes. Note that for brevity, a separate image for each individual case is not provided but rather results of similar character (i.e. the same overall shape, location of primary breaks and general debris orientation) are referenced by a single schematic diagram.

Tables 2-6 show that in general, the lower the blast pressure, the less sensitive the results are to changes in material parameters. This is true for most of the parameters studied. Note that for some cases (for example those in Tables 4-6), the small sensitivity is in part because blast pressure is of a magnitude (very low or very high) such that parameters require a large amount of deviation from base values to reach a minimum threshold that would result in wall failure or wall survival (i.e. a change in failure mode).

The magnitude of sensitivity of results to each parameter is similar. It can also be said that there is an interaction between blast pressure and parameter sensitivity, as the parameter most influential on results varies with blast load. For the high pressure case,

failure mode is most sensitive to boundary block strength. The detailed modeling of the boundary condition is essential to capture the failure mode as shown in figure 4. At the moderate pressure cases (grouted), contact surface interaction also becomes relatively important, as compared to the reduced blast load, frictional forces are now of a magnitude that they may significantly influence failure shape. At the low pressure blasts, mortar strength becomes important, as this is the primary determinant of wall failure or survival (whereas for the higher blast loads, failure occurs regardless of mortar strength).
The results also indicate that, for lower blast pressures, if parameter adjustments do result in behaviors that not correct, fewer variations of this incorrect behavior are displayed. Compare the many different 'incorrect' grouted results in Tables 1 and 2 to the few in Table 4, for example. For the former, correct results are inherently more sensitive to parameters.

Note that primary debris velocity is not particularly sensitive to parameter values nor mode failure shape. As this measure is used as the primary determinant of building occupant injury, the consistency of this measure for various parameters (and thus its potential predictability) is a fortunate finding.

An important result to observe that enhances the usefulness of the model is that adjusting parameters arbitrarily will not produce the failure mode desired for any blast pressure case. For example, notice in the tables that the high-pressure failure mode (figures 4, 14) cannot be reproduced by any parameter adjustment at moderate or lower blast pressures. Similarly, the failure case for moderate pressure, grouted walls (figures 5, 15) cannot be reproduced by either the high pressure (Table 2) or low pressure (Table 4) grouted cases, regardless of parameter values. It is also generally not possible, unless

extreme parameter values are used, to obtain a wall failure for a case that actually did not fail, and vice-versa. It should be noted that various combinations of parameter adjustment were studied as well (i.e. adjusting multiple parameters simultaneously), with similar results.

The real value of a model is its ability to predict experimental data rather than matching results by adjusting parameters for each case. The model has shown to be sensitive to the material properties of the CMU blocks. To fully demonstrate the validity of the model, then, this material information is needed. Unfortunately, experimental data for the failure strengths of the actual top block CMU's used in the wall, as well as their kinetic friction coefficients, are not available. Therefore, at present, it is not certain that CMU walls subjected to blast loads can be definitively modeled with this technique (or currently, any other). However, the following observations are offered:

1) In general it is not possible to reproduce a failure mode associated with a particular blast load category using a different blast load category, with any measure of parameter adjustment. Thus, as shown in the sensitivity study, for a given blast load, it is not possible to adjust input parameters and obtain any failure mode that is desired. In fact, a particular set of input parameters for a particular load case will typically result in either the correct failure mode being obtained for the associated experimental test or a failure mode incorrect for any of the tests.

2) It is likely that the sensitivity of wall behavior to CMU properties is an actual phenomenon and not modeling error. This is suggested by reports of nearly identical CMU wall blast tests giving significantly different behavior results (Dennis 2000). This is not surprising, considering the high degree of variation in typical CMU material

parameters, as well as wall construction. For example, when measuring the modulus of rupture of CMU walls subjected to a uniform static pressure load, an industry report found coefficients of variation (COV) as high as 72% for construction similar to the test specimens used in this study (NCMA 1994) (for comparison, rolled structural steel yield COV is about 5% (Nowak and Collins 2000)). Beall (1993) reports a typical variation of compressive strength of the CMU's used in this study from 12.4 to 19.3MPa (an indication of failure pressure), while nominal mortar strength (an indicator of slide-line strength) in controlled situations are reported to typically vary by 40% (ASTM 1989). The large variation that may be expected in interface friction was reported above. These data do not include additional variations due to strain rate strengthening effects.

3) The computational model can replicate experimental results if material parameters are set within this reasonably expected range of variation.

Due to the apparent blast-response sensitivity of CMU walls to material parameters, combined with the high typical variation of these parameters, it is unlikely that the development of an accurate model using nominal material parameters for all cases is possible. Clearly, further verification is needed of this and other modeling efforts, although the necessary data are often unavailable. In lieu of using actual CMU material data, considering the large variations in CMU properties, a stochastic approach to wall analysis, where failure is measured probabilistically rather than deterministically, may be viable.

CONCLUSIONS

Fourteen CMU walls subjected to various blast pressures were analyzed with the finite element method, with the goal of developing a computationally-efficient but accurate model. The walls can be grouped into three modes of failure, which correspond to three ranges of blast pressures. Modeling the problem is complex, requiring a highly nonlinear, large strain, large displacement approach that allows arbitrary element contact and separation. Previous models applied to this problem (DOE 1992; Forsen 1985; Bogosian 1997; Murray 1997; Dennis et al. 2001) could not reliably model wall failure nor wall failure mode. The technique developed in this study can correctly model which walls will fail and which will not. It can replicate wall failure mode at high blast pressure if appropriate material constants for the top CMU block are chosen. Here, further experimental data are needed to verify the numerically predicted sensitivity of failure mode to top block material parameters. Due to significant variations in material properties and wall construction, it seems unlikely that the development of an accurate model using average material parameters for all cases is possible. Given the high variability in material properties of CMU walls, a stochastic approach to wall analysis may be more appropriate. To this end, additional experimental and computational research on this important subject is called for.

ACKNOWLEDGMENTS

This research was conducted for the U.S. Army Engineer Research and Development Center. The authors gratefully acknowledge permission from the Chief of Engineers to publish this paper.

REFERENCES

ACI 318-95 (1995). "Building Code Requirements for Structural Concrete." American Concrete Institute.

ACI 530-95/ASCE 5-95/TMS 402-95. (1995). "Building Code Requirements for Masonry Structures." American Concrete Institute.

ASTM C 270-89. (1989). "Standard Specification for Mortar for Unit Masonry. American Society for Testing and Materials.

Baylot, J. T., Woodson, S.C., O'Daniel, J.L., and Bullock, W. (2001). "Analysis and Retrofit of CMU Walls." Proceedings of 2001 ASCE Structures Congress, May 21-23, Washington, D.C.

Beall, C. (1993). "Masonry design and detailing." McGraw Hill, New York.

Bogosian, D.D. (1997). "Validation of component vulnerability curves for unfilled masonry in-fill walls and steel joints, Rep. TR-96-30.2. " Karagozian & Case, Glendale, CA.

Dennis, S.T. (2000). "Masonry Walls Subjected to Blast Loading, Technical Report SL-00-2000." US Army Corps. of Engineers, Waterways Experiment Station.

Dennis, S.T., Baylot, J.T., and Woodson, S.C. (2001). "Response of 1/4-Scale Concrete Masonry Unit (CMU) Walls to Blast." ASCE Journal of Engineering Mechanics, Vol 128 No. 2, pp 134-142.

DOE/TIC 11268 (1992). "A manual for the prediction of blast and fragment loadings on structures." US Department of Energy.

Flanagan, D.P. and Belytschko, T. (1981). "A Uniform Strain Hexahedron and Quadrilateral and Orthogonal Hourglass Control. International Journal of Numerical Methods in Engineering," V 17, pp 679-706.

Forsen, R. (1985). "Airblast loading of wall panels, FOA Rep. C 20586-D6." National Defense Research Institute, Stockholm, Sweden.

Lawrence Livermore National Laboratory (1999). "DYNA3D A nonlinear, explicit , three-dimensional finite element code for solid and structural mechanics-user manual."

Murray, Y.D. (1997). "Composite retrofit techniques for blast resistance, Rep. DSWA-TR-97-00." Defense Threat Reduction Agency, Dulles, VA.

National Concrete Masonry Association (1994). "Research Evaluation of the Flexural Tensile Strength of Concrete Masonry, Project # 93-172."

Nowak, A.S. and Collins, K. (2000). "Reliability of Structures." McGraw Hill, New York.

Seely, F.B. and Ensign, N.E. (1926) "Analytical Mechanics for Engineers." John Wiley and Sons, New York.

Virdee, A. (1990). " Fundamentals of reinforced masonry design." Professional Publications, Belmont California, 1990.

FIGURE CAPTIONS

1. Typical CMU Block

2. Experimental Set-up

3. Typical Blast Pressure and Impulse Curve

4. Typical 3-Piece Failure Mode, High Pressure Case

5. Typical 2-Piece Failure Mode, Fully-Grouted Wall, Moderate Pressure

6. Typical Moderate Pressure Failure Mode, Ungrouted Wall, Moderate Pressure

7. Typical Remaining Deformation in Unfailed Wall

8. Typical Impulse curves obtained from the different pressure gauges for a single test.

9. FE Model of Wall

10. CMU Discretization

11. CMU Material Model

12. Strain Rate Strengthening Curve

13. FE Model of Top CMU Block

14. Typical FE Model of High Pressure Case

15. Typical FE Model of Moderate Pressure Case, Grouted Wall

16. Typical FE Model of Moderate Pressure Case, Ungrouted Wall

17. Typical FE Model of Low Pressure Case

18. Debris Velocity (ft/sec) at ¼ Height and ½ Height of Wall

19. Alternate Failure Modes

TABLES

Figure 1. Typical CMU Block

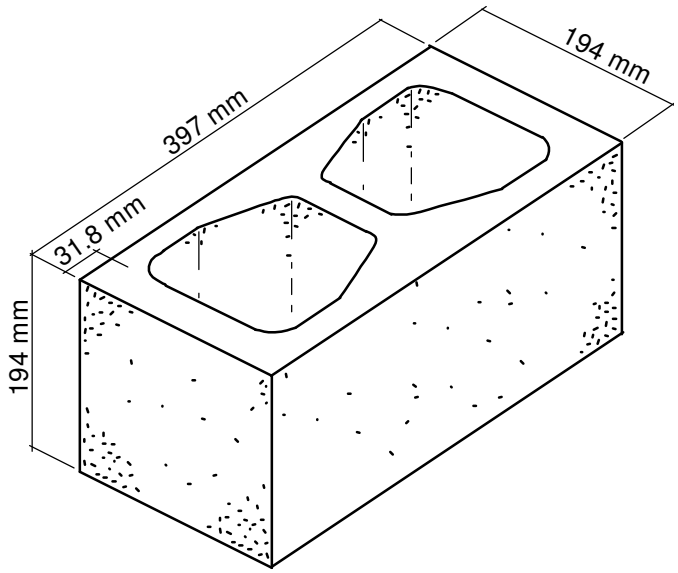

Figure 2. Experimental Set-up. Pressure gauges are the four small white circles on frame outer perimeter; one on top and two on each side (fifth hidden by test placard in lower left corner).

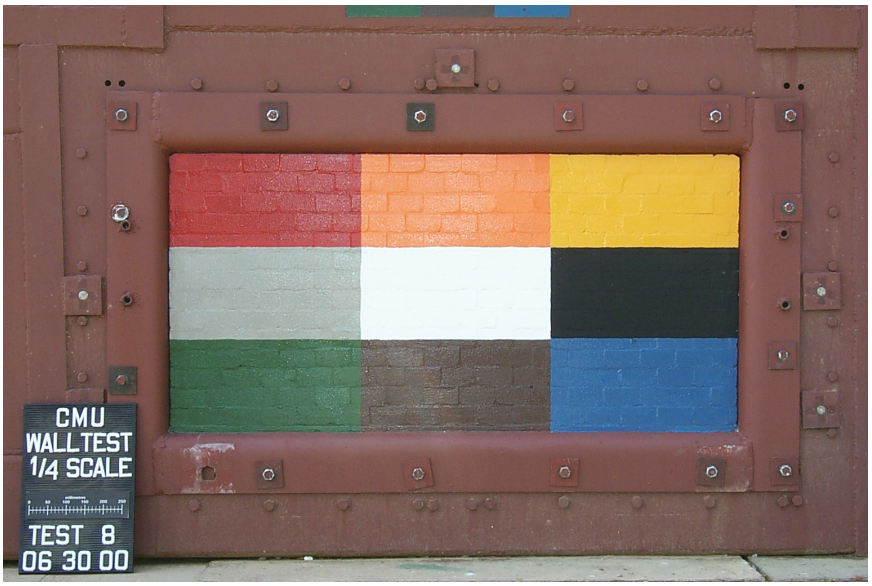

Figure 3. Typical Blast Pressure and Impulse Curve

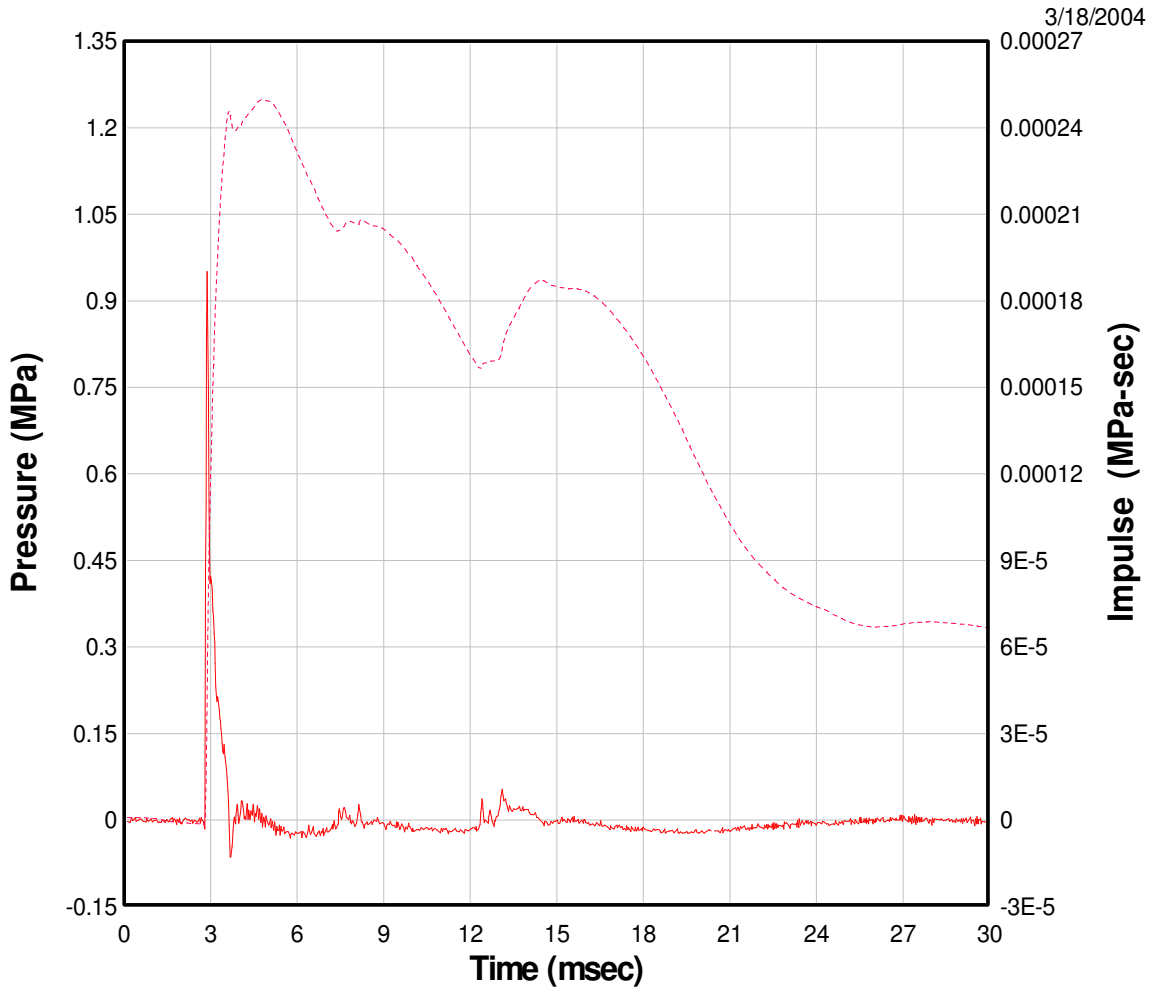

Figure 4. Typical 3-Piece Failure Mode, High Pressure

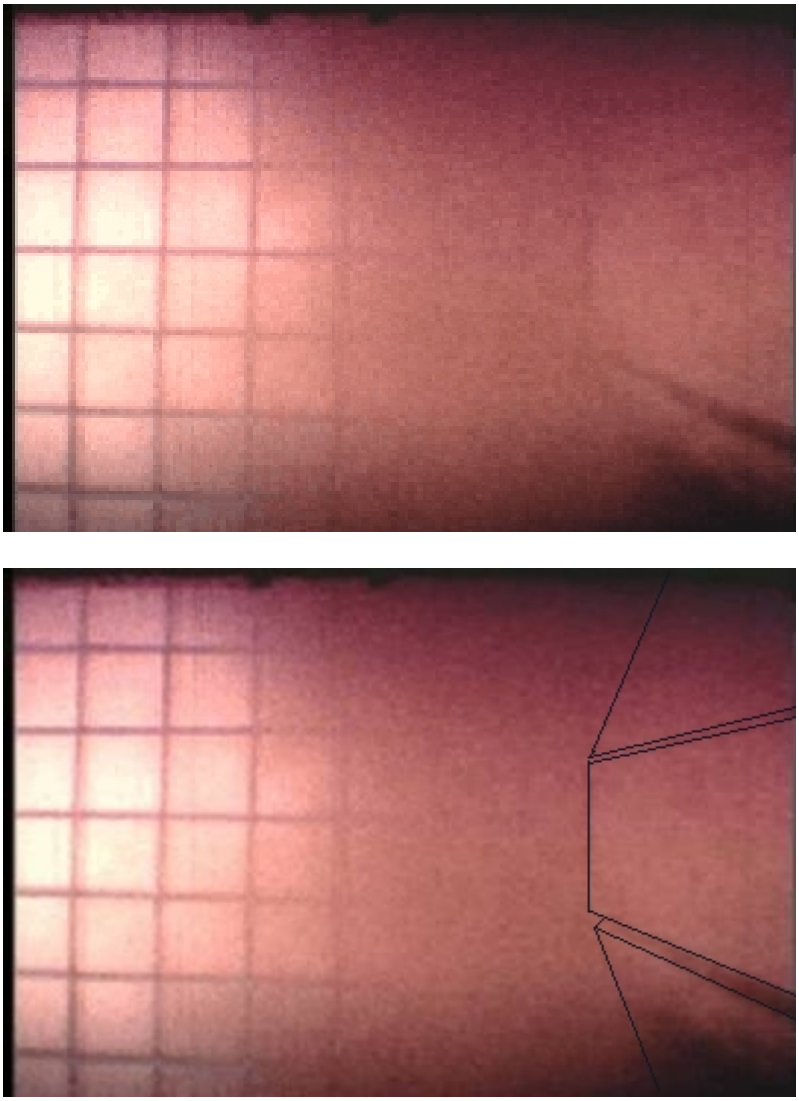

Figure 5. Typical 2-Piece Failure Mode, Fully-Grouted Wall, Moderate Pressure

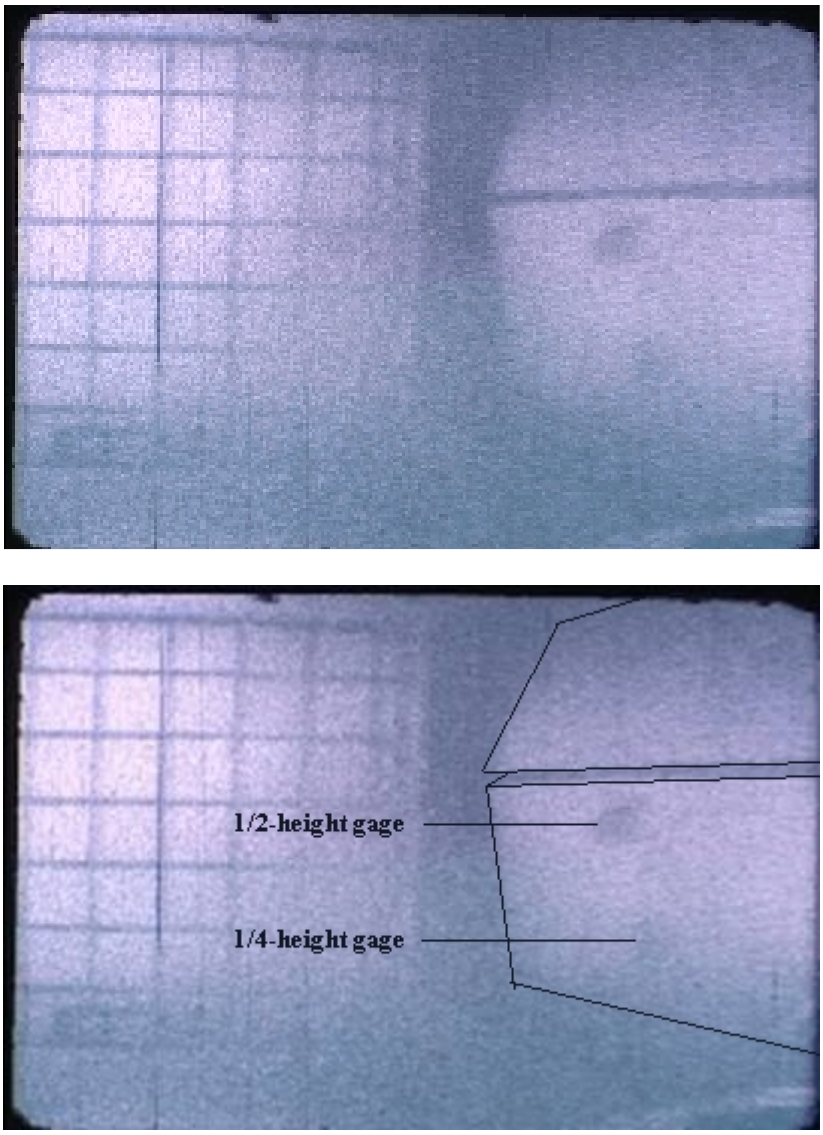

Figure 6. Typical Joint Separation Failure Mode, Ungrouted Wall, Moderate Pressure

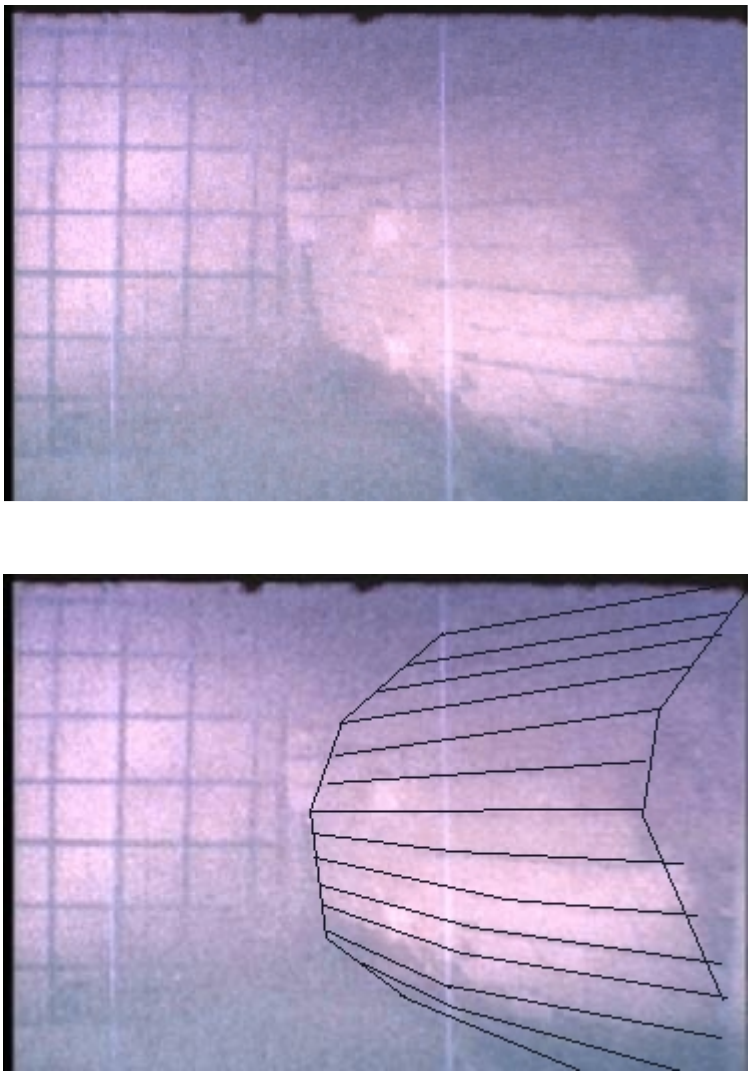

Figure 7. Typical Remaining Deformation in Unfailed Wall, Low Pressure

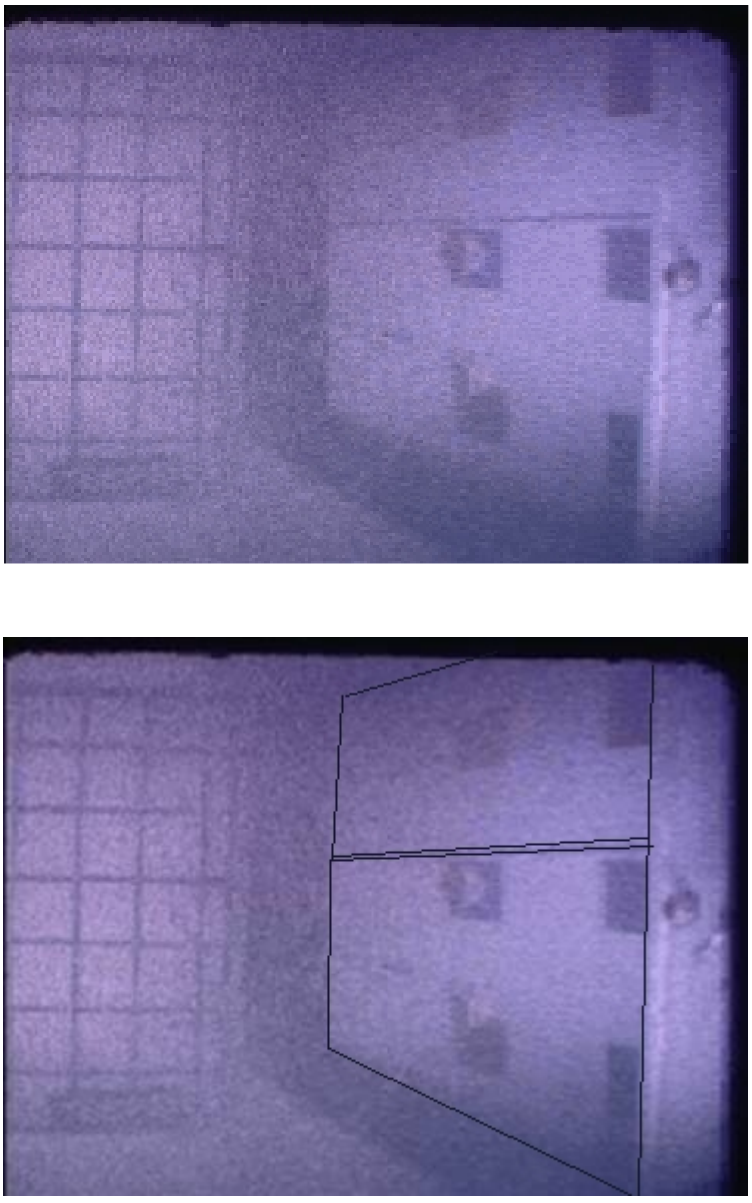

Figure 8. Typical Pressure and Impulse curves obtained from the different pressure gauges for a single test.

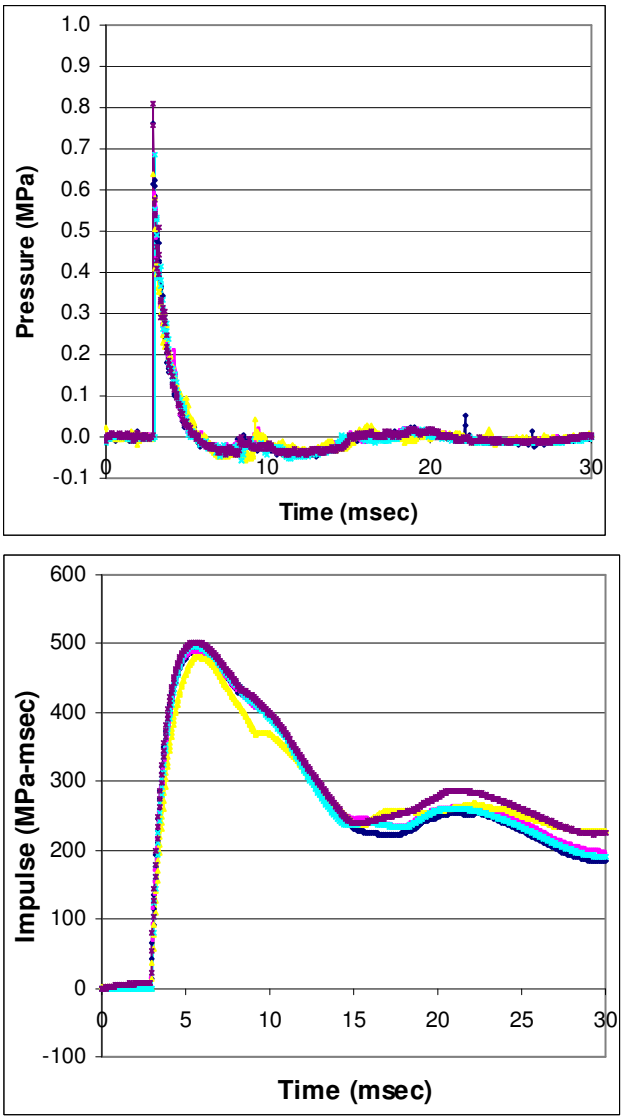

9. FE Model of Wall

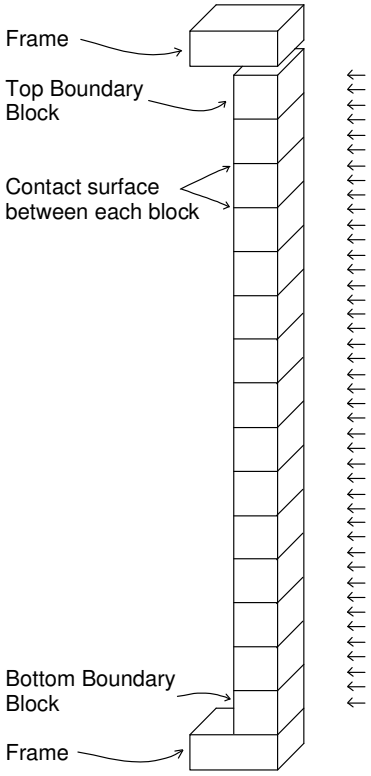

10. CMU Discretization

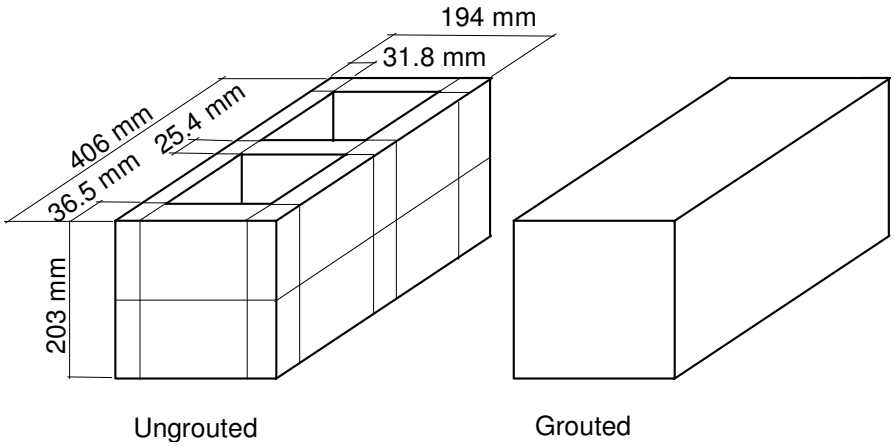

11. CMU Material Model

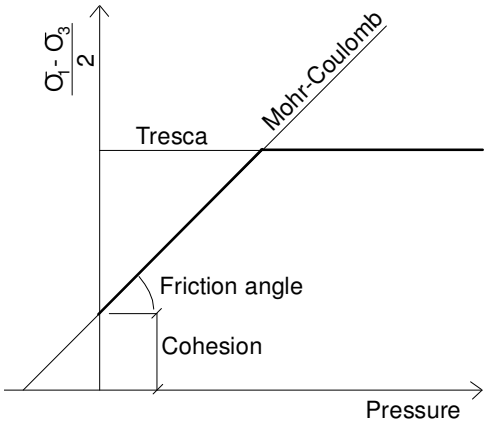

Figure 12. Strain Rate Strengthening Curve

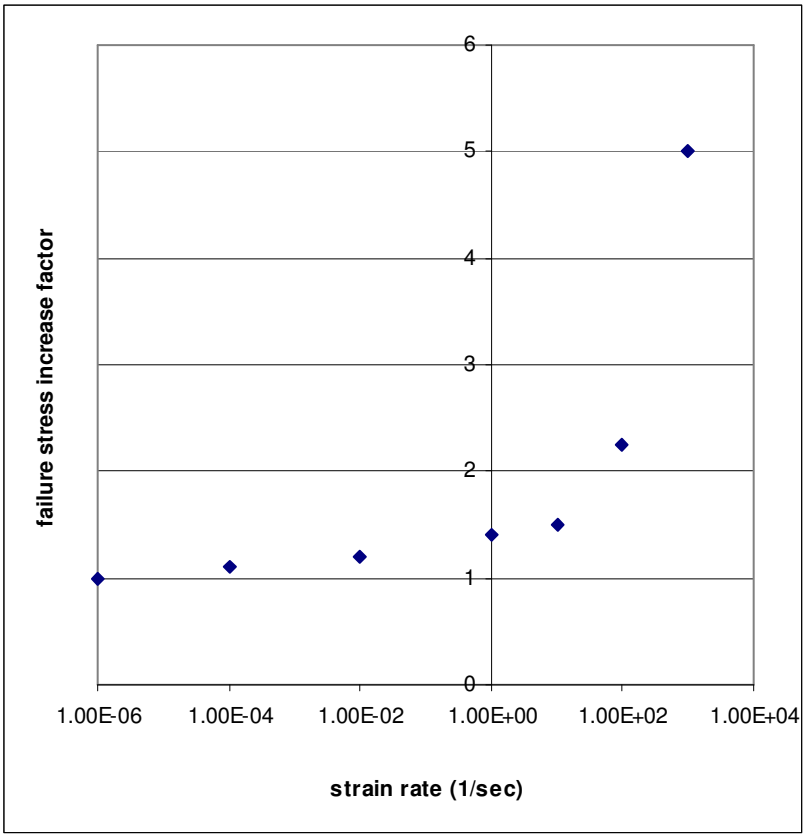

13. FE Model of Top CMU Block

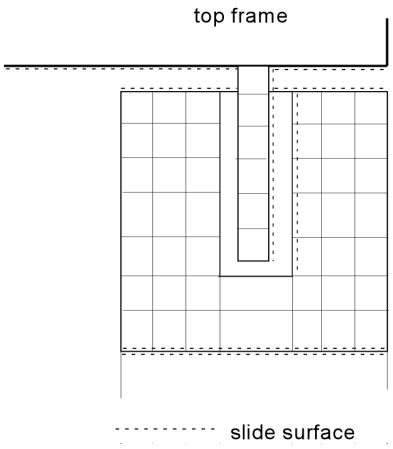

Figure 14. Typical FEA Result, High Pressure Case

Figure 15. Typical FEA Result, Moderate Pressure Case, Grouted

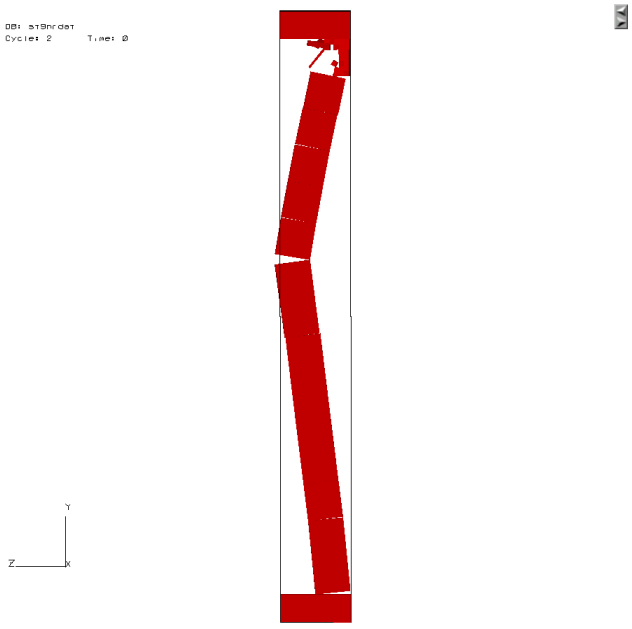

Figure 16. Typical FEA Result, Moderate Pressure Case, Ungrouted

Figure 17. Typical FEA Result, Low Pressure Case (in fully deformed state)

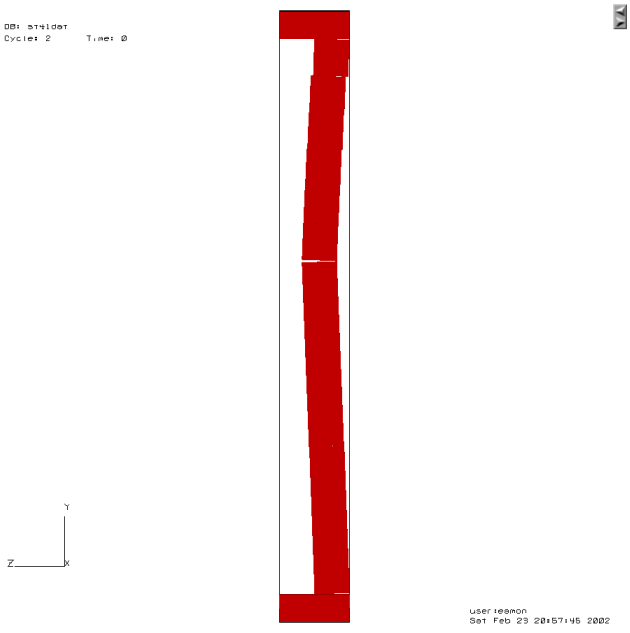

Figure 18. Debris Velocity (ft/sec) at ¼ Height and ½ Height of Wall

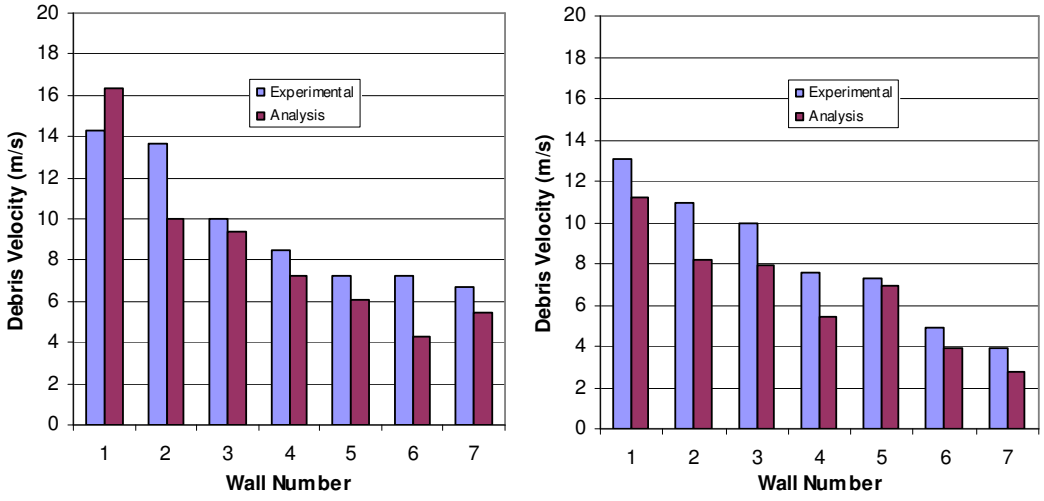

Figure 19. Alternate Failure Modes

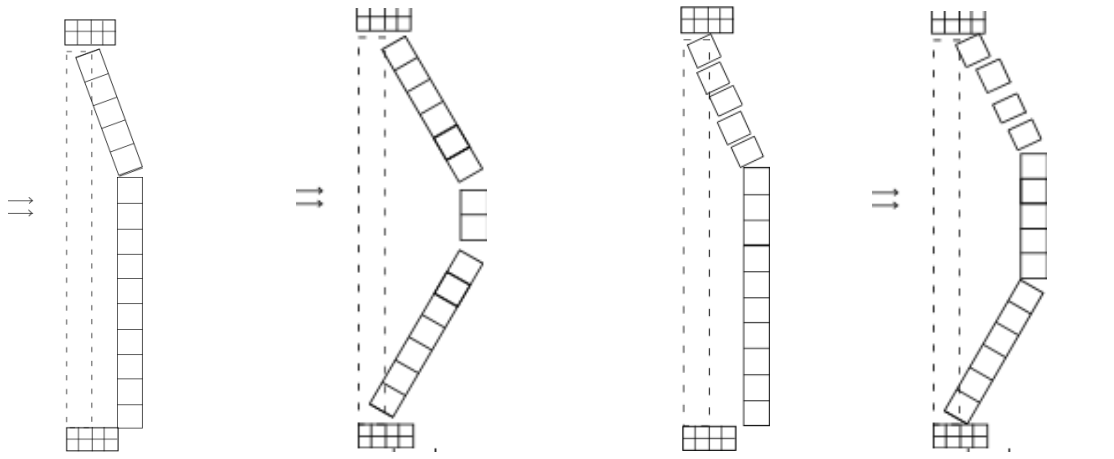

(a) (b) (c) (d)

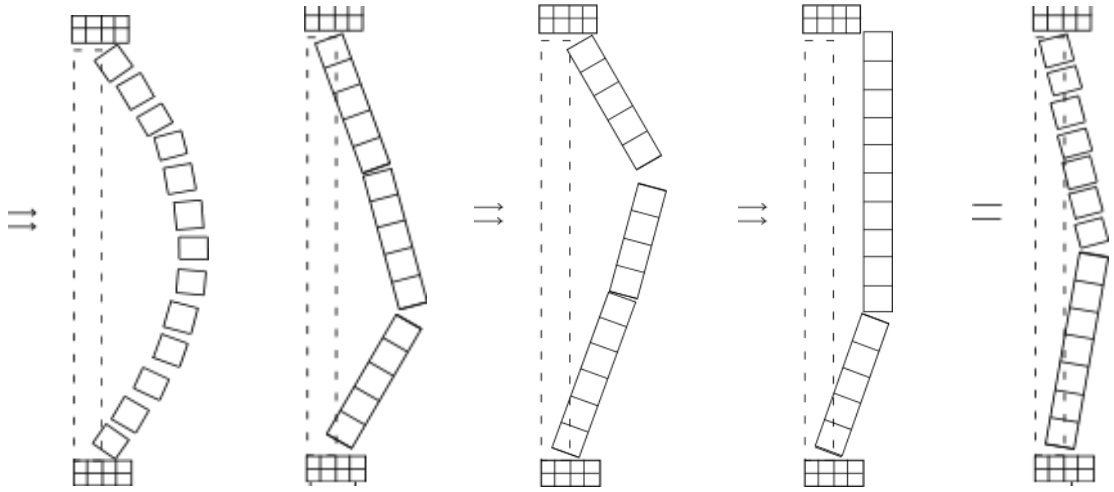

(e) (f) (g) (h) (i)

TABLE 1. Range of Model Parameters

Test Case	Frame (Boundary) Block	
	Friction	Failure Strength (kPa)
High Pr. (full grout)	0.50-0.65	6,500-9,000
Mod Pr. (full grout)	0.65-0.75	7,000-10,000
Mod. Pr. (ungrouted)	0.65-0.70	6,500-9,000
Low Pr. (full grout)	0.65*	9,000
Low Pr. (ungrouted)	0.65-0.70	7,500-9,500

*a value of 0.50 also worked well for all walls in this category

TABLE 2. High Pressure, Full Grout Case

Normalized Parameter	Failure Mode (see reference figure)	Debris Velocity (m/s) ½ ht.	¼ ht
Block Strength			
0.50	fig. 14	9.7	7.9
0.85-0.95	fig. 19a	9.4	9.1
0.97-1.03	CORRECT (fig. 14)	9.7-10*	7.9-8.2*
1.05-1.15	fig. 19b	9.7-10.3*	8-8.2*
1.50	fig. 19c	10.2	9.4
Frame Friction			
0.50	fig. 19a	10.6	10.2
0.70	fig. 19d	10.6	7.6
0.80-1.05	CORRECT (fig. 14)	10.5-10**	7.9-8.3*
1.10-1.50	fig. 19e	10.6-12.1*	7.3-9.1*
Mortar Strength			
0.50	fig. 19e	10.3-10**	7.7-7.6**
0.95-1.05	CORRECT (fig. 14)	10-10.2*	8.2
1.10	fig. 19f	9.7	9.1
1.15	fig. 19d	10	7.6
1.50	fig. 19g	10	8.2
Block Friction			
0.50	fig. 19c	10	8.2
0.80	fig. 19e	10.3	7.9
0.95-1.20	CORRECT (fig. 14)	10-10.3*	8.2-7.3**
1.30	fig. 19d	7.6	10.6
Blast Pressure			
0.80-0.90	fig. 19b	10-10.3*	3.9-4.5*
0.95-1.05	CORRECT (fig. 14)	9.7-10.2*	8-8.2*
1.10-1.20	fig. 19e	9.4-10.6*	10-11.2*

*debris velocity increases as parameter value increases
**debris velocity decreases as parameter value increases
***no obvious relationship between debris velocity and parameter value

TABLE 3. Moderate Pressure, Full Grout Case

Normalized Parameter	Failure Mode (see reference figure)	Debris Velocity (m/s) ½ ht.	¼ ht.
Block Strength			
0.50	fig. 19h	4.8	2.1
0.70	fig. 19i	4.8	1.8
0.80	fig 19a	4.8	2.4
0.90-1.05	CORRECT (fig. 15)	4.8	1.5-2.1
1.10-1.50	no failure	0	0
Frame Friction			
0.50-0.90	fig. 19a	3.9	1.8-2.1*
0.95-1.05	CORRECT (fig. 15)	4.8-3.9**	1.7-2.7**
1.10-1.50	no failure	0	0
Mortar Strength			
0.50	fig. 19e	5.8	3.6
0.80-1.20	CORRECT (fig. 15)	5.2-3.8**	1.7-2.1**
1.50	no failure	0	0
Block Friction			
0.50	no failure	0	0
0.90	fig. 19e	3.9	3.0
0.95-1.1	CORRECT (fig. 15)	4.5-4.8*	1.5-1.7*
1.2-1.5	fig. 19h	3.9	1.8-1.7**
Blast Pressure			
0.80-0.90	no failure	0	0
0.95-1.1	CORRECT (fig. 15)	4.2-4.8*	1.7-3.0*
1.2	fig. 19a	4.8	4.5

*debris velocity increases as parameter value increases
**debris velocity decreases as parameter value increases
***no obvious relationship between debris velocity and parameter value

TABLE 4. Low Pressure, Full Grout Case

Normalized Parameter	Failure Mode (see reference figure)	Debris Velocity (m/s) ½ ht.	¼ ht.
Block Strength			
0.50-1.50	CORRECT (no failure)	0	0
Frame Friction			
0.50-0.80	fig. 19h	2.1-2.4*	1.2-1.7*
0.90-1.50	CORRECT (no failure)	0	0
Mortar Strength			
0.50-1.05	CORRECT (no failure)	0	0
1.10-1.50	fig. 19h	1.8-1.5**	1.4-1.2**
Block Friction			
0.50-1.50	CORRECT (no failure)	0	0
Blast Pressure			
0.80-1.10	CORRECT (no failure)	0	0
1.20	fig. 19h	2.7	1.8

*debris velocity increases as parameter value increases
**debris velocity decreases as parameter value increases
***no obvious relationship between debris velocity and parameter value

TABLE 5. Moderate Pressure, Ungrouted Case

Normalized Parameter	Failure Mode (see reference figure)	Debris Velocity (m/s) ½ ht.	¼ ht.
Block Strength			
0.50-1.50	CORRECT (fig. 16)	12.1-16.7*	7-8.2*
Frame Friction			
0.50	fig. 19a	13.3	11.8
0.75-1.10	CORRECT (fig. 16)	14.2-13.3**	9.1-7.9**
1.20-1.50	fig. 15	13	7.6
Mortar Strength			
0.50-1.50	CORRECT (fig. 16)	13.6-17*	7.9-9.7***
Block Friction			
0.50-1.50	CORRECT (fig. 16)	13-18.2*	7.6-8.2***
Blast Pressure			
0.5	fig. 15	11.5	5.8
0.7-1.5	CORRECT (fig. 16)	12.1-16.7*	7.9-9.4*

*debris velocity increases as parameter value increases

**debris velocity decreases as parameter value increases

***no obvious relationship between debris velocity and parameter value

TABLE 6. Low Pressure, Ungrouted Case

Normalized Parameter	Failure Mode (see reference figure)	Debris Velocity (m/s) ½ ht.	¼ ht.
Block Strength			
0.50	fig. 15	2.7	1.5
0.60	fig. 19e	3.3	2.4
0.70-1.50	CORRECT (no failure)	0	0
Frame Friction			
0.50	fig. 19h	35	3
0.75-1.50	CORRECT (no failure)	0	0
Mortar Strength			
0.50	fig. 19e	3.9	2.1
0.80-1.50	CORRECT (no failure)	0	0
Block Friction			
0.50	large deformation, but no failure	0	0
0.60-1.50	CORRECT (no failure)	0	0
Blast Pressure			
0.5-1.1	CORRECT (no failure)	0	0
1.5	fig. 15	5.5	2.4